Progress In Electromagnetics Research M, Vol. 82, 49–59, 2019

Spatial and Polarization Angle Estimation of Mixed-Targets in MIMO Radar

Srinivasarao Chintagunta[1, *] and Palanisamy Ponnusamy[2]

Abstract—This paper proposes an approach for estimating the spatial and polarization angles of mixed-targets in bistatic MIMO radar. Mixed-targets mean the combination of uncorrelated, partially correlated, and groups of coherent targets. The approach resolves rank deficiency of received signal covariance matrix and then exploits the ESPRIT-based method for estimating the angles of direction-of-departure (DOD) and direction-of-arrival (DOA). This paper also presents an analytical review and necessary conditions for resolving the rank deficiency under various scenarios of the MIMO radar. Simulation results show the effectiveness of the proposed approach.

1. INTRODUCTION

Multiple-input multiple-output (MIMO) radar has been receiving much attention for localization of the targets over the conventional phased array radar [1]. For localization of the targets, direction estimation is a key issue and has found many investigations in the literature [2–9]. Majority of these investigations focus on the estimation of direction-of-departure (DOD) and direction-of-arrival (DOA) of uncorrelated targets [2–7] and coherent targets [8, 9]. Two-dimensional (2D) DOD and 2D-DOA estimation have also been investigated for the case of uncorrelated targets [10–12]. 2D means azimuth and elevation angles of a target. The 2D DOD/DOA estimation is important specifically when the targets are resolvable in azimuth angles but not resolvable in elevation angles, and vice-versa.

Moreover, in a stringent scenario where the targets are closely spaced and cannot be resolvable with spatial angles, the polarization estimation may be required for localizing and distinguishing the targets. Though the estimation of signal parameters via rotational invariance technique (ESPRIT) based method in [12] estimates both spatial and polarization angles, estimation performance is shown only for the spatial angles. However, this ESPRIT-based method fails under the coherent target scenario due to the rank deficiency of received signal covariance matrix. In practice, the received signals are coherent or partially correlated or may be a combination of coherent and partially correlated [13–15]. Therefore, in this paper, we formulate a model for mixed targets which are the combination of uncorrelated, partially correlated, and groups of coherent targets, and estimate both spatial and polarization angles. The methodology of this paper resolves the rank deficiency of mixed targets using spatial smoothing and then estimates the angles employing the ESPRIT-based method [12]. This paper also presents an analytical discussion and necessary conditions of the smoothing for decorrelating the mixed targets under different scenarios of the MIMO radar.

Notation: Vectors and matrices are represented by lowercase and uppercase bold characters, respectively. $(\cdot)^T$ denotes the transpose, and $(\cdot)^H$ indicates the conjugate-transpose. Symbols $\otimes$, $\odot$, and $\oplus$ denote the Kronecker product, Khatri-Rao product, and Hadamard product, respectively. $\mathbf{I}_n$, $0_{m\times n}$, and 0_n denote $n \times n$ identity matrix, $m \times n$ zeros matrix, and $n \times n$ zeros matrix, respectively. In particular, diag$\{\cdot\}$ and blkdiag$\{\cdot\}$ represent the diagonal matrix and block diagonal matrix, respectively. $[\mathsf{J}]_{k,k}$ selects the entry in the kth row and kth column of matrix J.

Received 17 April 2019, Accepted 5 June 2019, Scheduled 20 June 2019

* Corresponding author: Srinivasarao Chintagunta (srinivasarao@iiit-bh.ac.in).

[1] International Institute of Information Technology, Bhubaneswar, India. [2] National Institute of Technology, Tiruchirappalli, India.

2. SIGNAL MODEL

Consider a bistatic MIMO radar that comprises uniform linear arrays of M electromagnetic vector sensors (EVSs) and N EVSs at the transmitter and receiver, respectively. Each EVS consists of three orthogonally oriented electric-dipoles and three orthogonally oriented magnetic-loops. The inter-sensor spacing of the transmit array is d_{t}, and the receive array is d_{r}. Suppose that there are K targets present in the same range cell. Then, deploying the arrays along the y-axis, steering vectors of the transmit array $\mathbf{a}_{\mathrm{t}}$ and receive array $\mathbf{a}_{\mathrm{r}}$ towards the kth target direction can be expressed as

$$\begin{aligned}\mathbf{a}_{\mathrm{t}_k} &= \mathbf{b}_{\mathrm{t}_k}(\theta_{\mathrm{t}_k}, \phi_{\mathrm{t}_k}) \otimes \mathbf{c}_{\mathrm{t}_k}(\theta_{\mathrm{t}_k}, \phi_{\mathrm{t}_k}, \gamma_{\mathrm{t}_k}, \eta_{\mathrm{t}_k}) \\ \mathbf{a}_{\mathrm{r}_k} &= \mathbf{b}_{\mathrm{r}_k}(\theta_{\mathrm{r}_k}, \phi_{\mathrm{r}_k}) \otimes \mathbf{c}_{\mathrm{r}_k}(\theta_{\mathrm{r}_k}, \phi_{\mathrm{r}_k}, \gamma_{\mathrm{r}_k}, \eta_{\mathrm{r}_k})\end{aligned} \tag{1}$$

where $\mathbf{b}_{\mathrm{t}_k} = [1, \alpha_k, \ldots, \alpha_k^{M-1}]^T$ in which $\alpha_k = e^{-j2\pi d_{\mathrm{t}} \sin\theta_{\mathrm{t}_k} \sin\phi_{\mathrm{t}_k}/\lambda}$ with λ being the wavelength, and $\mathbf{b}_{\mathrm{r}_k} = [1, \beta_k, \ldots, \beta_k^{N-1}]^T$ in which $\beta_k = e^{-j2\pi d_{\mathrm{r}} \sin\theta_{\mathrm{r}_k} \sin\phi_{\mathrm{r}_k}/\lambda}$. $\mathbf{c}_{\mathrm{t}_k}/\mathbf{c}_{\mathrm{r}_k}$ denotes the spatial response vector of the transmitting/ receiving EVS. The subscript $\mathrm{t}_k/\mathrm{r}_k$ indicates that the concerning parameter or vector belonging to the transmitter/receiver associated with the kth target. Thus, the spatial response vector $\mathbf{c}_i, i = \mathrm{t}_k, \mathrm{r}_k$, of an EVS can be expressed as

$$\mathbf{c}_i = \mathbf{F}(\theta_i, \phi_i)\mathbf{g}(\gamma_i, \eta_i) = \begin{bmatrix} \cos\theta_i \cos\phi_i & -\sin\phi_i \\ \cos\theta_i \sin\phi_i & \cos\phi_i \\ -\sin\theta_i & 0 \\ -\sin\phi_i & -\cos\theta_i \cos\phi_i \\ \cos\phi_i & -\cos\theta_i \sin\phi_i \\ 0 & \sin\theta_i \end{bmatrix} \begin{bmatrix} \sin\gamma_i e^{j\eta_i} \\ \cos\gamma_i \end{bmatrix} \tag{2}$$

where $\phi_i \in [0, 2\pi)$, $\theta_i \in [0, \pi)$, $\gamma_i \in [0, \pi/2)$, and $\eta_i \in [-\pi, \pi)$ respectively denote the azimuth angle, elevation angle, auxiliary polarization angle, and the polarization phase difference of the concerning target (i.e., $i = \mathrm{t}_k, \mathrm{r}_k$).

Assume that the elements of the transmit-array transmit orthogonal coded vector signals $\mathbf{V} = [\mathbf{v}_{1,1}, \ldots, \mathbf{v}_{1,6}, \ldots, \mathbf{v}_{M,1}, \ldots, \mathbf{v}_{M,6}]^T$, where $\mathbf{v}_{m,i}$ denotes the $P \times 1$ coded vector signal by the ith element of the mth EVS. The transmitted signals are reflected at K far-field targets. Then the received signal at the lth snapshot can be expressed as

$$\mathbf{X}(l) = \sum_{k=1}^{K} \mathbf{a}_{\mathrm{r}_k} s_k(l) \mathbf{a}_{\mathrm{t}_k}^T \mathbf{V} + \mathbf{W}(l) \tag{3}$$

In practice, vectorization of the output of matched filters matched to the transmission signal is used for processing the signal [5, 6]. The output of the matched filter bank is represented by $\mathbf{X}_{\mathrm{out}}(l) = \mathbf{X}(l)\mathbf{V}^H/\sqrt{P}$. Then the vectorization of $\mathbf{X}_{\mathrm{out}}(l)$ can be expressed as [12]

$$\mathbf{y}(l) = \mathrm{vec}(\mathbf{X}_{\mathrm{out}}(l)) = \sum_{k=1}^{K} (\mathbf{a}_{\mathrm{t}_k} \otimes \mathbf{a}_{\mathrm{r}_k}) \sqrt{P} s_k(l) + \mathbf{z}(l) = \mathbf{A}\mathbf{s}(l) + \mathbf{z}(l) \tag{4}$$

where $\mathbf{A} = [\mathbf{a}_{\mathrm{t}_1} \otimes \mathbf{a}_{\mathrm{r}_1}, \ldots, \mathbf{a}_{\mathrm{t}_K} \otimes \mathbf{a}_{\mathrm{r}_K}]$, $\mathbf{s}(l) = [\sqrt{P}s_1(l), \ldots, \sqrt{P}s_K(l)]^T$ denotes the reflectivity vector at output of the matched filters, and $\mathbf{z}(l) = \frac{1}{\sqrt{P}}\mathrm{vec}(\mathbf{W}(l)\mathbf{V}^H)$ is the output noise vector.

3. PROPOSED APPROACH

3.1. Problem Formulation

In a practical scenario, as the model shown in Fig. 1, the nonzero reflectivities $\{s_k(l)\}_{k=1}^K$ are the combination of uncorrelated, partially correlated, and groups of coherent. Without loss of generality, assume that the first K_{u} targets (in fact, target reflectivities) are uncorrelated, next K_{p} targets partially correlated, and the remaining are D clusters of $K_{\mathrm{c}} = \sum_{d=1}^{D} Q_d = K - K_{\mathrm{u}} - K_{\mathrm{p}}$ coherent targets, where Q_d denotes the number of coherent targets in dth cluster. Further, assume that the targets in one cluster

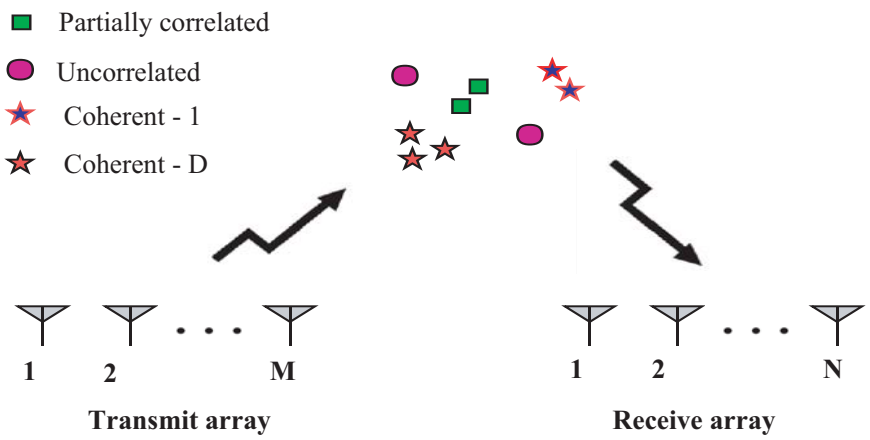

Figure 1. Model map of the scenario considered in problem formulation.

are coherent and uncorrelated with the targets in other clusters as well as K_{u} uncorrelated targets and K_{p} partially correlated targets. Under this scenario, the signal model in Eq. (4) can be written as

$$\mathbf{y}(l) = \mathbf{A}_{\mathrm{u}}\mathbf{s}_{\mathrm{u}}(l) + \mathbf{A}_{\mathrm{p}}\mathbf{s}_{\mathrm{p}}(l) + \mathbf{A}_{\mathrm{c}}\mathbf{s}_{\mathrm{c}}(l) + \mathbf{z}(l) = [\mathbf{A}_{\mathrm{u}},\ \mathbf{A}_{\mathrm{p}},\ \mathbf{A}_{\mathrm{c}}] \begin{bmatrix} \mathbf{s}_{\mathrm{u}}(l) \\ \mathbf{s}_{\mathrm{p}}(l) \\ \mathbf{s}_{\mathrm{c}}(l) \end{bmatrix} + \mathbf{z}(l) \tag{5}$$

where $\mathbf{A}_{\mathrm{u}} = [\mathbf{a}_{\mathrm{t}_1} \otimes \mathbf{a}_{\mathrm{r}_1}, \ldots, \mathbf{a}_{\mathrm{t}_{K_{\mathrm{u}}}} \otimes \mathbf{a}_{\mathrm{r}_{K_{\mathrm{u}}}}]$ represents the steering matrix of all uncorrelated targets; $\mathbf{A}_{\mathrm{p}} = [\mathbf{a}_{\mathrm{t}_{K_{\mathrm{u}}+1}} \otimes \mathbf{a}_{\mathrm{r}_{K_{\mathrm{u}}+1}}, \ldots, \mathbf{a}_{\mathrm{t}_{K_{\mathrm{u}}+K_{\mathrm{p}}}} \otimes \mathbf{a}_{\mathrm{r}_{K_{\mathrm{u}}+K_{\mathrm{p}}}}]$ denotes the steering matrix of all partially correlated targets, $\mathbf{A}_{\mathrm{c}} = [\mathbf{A}_{\mathrm{c}_1}, \ldots, \mathbf{A}_{\mathrm{c}_D}]$ in which $\mathbf{A}_{\mathrm{c}_d} = [\mathbf{a}_{\mathrm{t}_{d,1}} \otimes \mathbf{a}_{\mathrm{r}_{d,1}}, \ldots, \mathbf{a}_{\mathrm{t}_{d,Q_d}} \otimes \mathbf{a}_{\mathrm{r}_{d,Q_d}}]$, $d = 1, \ldots, D$, being the steering matrix concerning with all coherent targets in the dth cluster; $\mathbf{s}_{\mathrm{u}}(l) = [\sqrt{P}s_1(l), \ldots, \sqrt{P}s_{K_{\mathrm{u}}}(l)]^T$ denotes the reflectivity vector of uncorrelated targets; $\mathbf{s}_{\mathrm{p}}(l) = [\sqrt{P}s_{K_{\mathrm{u}}+1}(l), \ldots, \sqrt{P}s_{K_{\mathrm{u}}+K_{\mathrm{p}}}(l)]^T$ represents the reflectivity vector of all partially correlated targets; and $\mathbf{s}_{\mathrm{c}}(l) = [\mathbf{s}^T_{K_{\mathrm{u}}+K_{\mathrm{p}}+1}(l), \ldots, \mathbf{s}^T_{K_{\mathrm{u}}+K_{\mathrm{p}}+D}(l)]^T$ in which $\mathbf{s}_{K_{\mathrm{u}}+K_{\mathrm{p}}+d}(l)$ being the reflectivity vector of all coherent targets in dth cluster. Further, the coherent reflectivity vector $\mathbf{s}_{K_{\mathrm{u}}+K_{\mathrm{p}}+d}(l)$ can be decomposed as $\mathbf{s}_{K_{\mathrm{u}}+K_{\mathrm{p}}+d}(l) = \sqrt{P}s_{K_{\mathrm{u}}+K_{\mathrm{p}}+d}(l)\boldsymbol{\rho}_d$, where $s_{K_{\mathrm{u}}+K_{\mathrm{p}}+d}(l)$ is the common reflectivity of the dth cluster, and $\boldsymbol{\rho}_d = [\rho_{d,1}, \ldots, \rho_{d,Q_d}]^T$ denotes the complex coefficient vector of dth cluster. The coefficients in $\boldsymbol{\rho}_d$ represent the magnitude and phase relationship of Q_d coherent targets in the dth cluster.

Therefore, the covariance matrix of the signal $\mathbf{y}(l)$ in Eq. (5) is given by

$$\mathbf{R}_{\mathrm{y}} = \mathbb{E}\left[\mathbf{y}(l)\mathbf{y}(l)^H\right] = \mathbf{A}\mathbf{R}_{\mathrm{s}}\mathbf{A}^H + \mathbf{R}_{\mathrm{z}} \tag{6}$$

where $\mathbf{A} = [\mathbf{A}_{\mathrm{u}},\ \mathbf{A}_{\mathrm{p}},\ \mathbf{A}_{\mathrm{c}}]$, $\mathbf{R}_{\mathrm{s}} = \mathrm{blkdiag}\{\mathbf{R}_{\mathrm{u}}, \mathbf{R}_{\mathrm{p}}, \mathbf{R}_{\mathrm{c}}\}$ in which $\mathbf{R}_{\mathrm{u}} = \mathrm{diag}\{\sigma_1^2, \ldots, \sigma_{K_{\mathrm{u}}}^2\}$ is the covariance matrix of $\mathbf{s}_{\mathrm{u}}(l)$; $\mathbf{R}_{\mathrm{p}}$ is the covariance matrix of $\mathbf{s}_{\mathrm{p}}(l)$; $\mathbf{R}_{\mathrm{c}} = \mathrm{blkdiag}\{\mathbf{R}_{\mathrm{c}_1}, \ldots, \mathbf{R}_{\mathrm{c}_D}\}$ is the covariance matrix of $\mathbf{s}_{\mathrm{c}}(l)$; $\mathbf{R}_{\mathrm{c}_d}(d = 1, \ldots, D)$ denotes the covariance of $\mathbf{s}_{K_{\mathrm{u}}+K_{\mathrm{p}}+d}(l)$; and $\mathbf{R}_{\mathrm{z}}$ is the noise covariance matrix.

For mixed targets, the rank of $\mathbf{R}_{\mathrm{s}}$ is less than the number of targets present, and thus $\mathrm{rank}(\mathbf{R}_{\mathrm{y}}) < K$ under the noise-free condition. Consequently, the ESPRIT-based method in [12] fails to resolve the targets as the angle estimates of DODs and DOAs are inaccurate.

3.2. Construction of a Full-Rank Covariance Matrix

The spatial smoothing of the MIMO radar divides the transmit array and receive array into P_{t} and P_{r} numbers of uniformly overlapped subarrays, respectively. Each transmitting subarray comprises M_{t} EVSs, and each receiving subarray has N_{r} EVSs. Considering the maximum overlapping of the subarrays, we can obtain $P_{\mathrm{t}} = M - M_{\mathrm{t}} + 1$ and $P_{\mathrm{r}} = N - N_{\mathrm{r}} + 1$ numbers of subarrays. In fact, the arrays are not segmented physically, but the equivalent covariance matrices of these subarrays are obtained from the received signal covariance matrix in Eq. (6). Let the covariance matrix between

the mth ($m = 1, \ldots, P_\mathrm{t}$) transmitting subarray and the nth ($n = 1, \ldots, P_\mathrm{r}$) receiving subarray be denoted with $\mathbf{R}_\mathrm{y}^{[m,n]} \in \mathbb{C}^{36M_\mathrm{t}N_\mathrm{r} \times 36M_tN_\mathrm{r}}$. Then the subarrays covariance matrices $\mathbf{R}_\mathrm{y}^{[m,n]}$ can be obtained from $\mathbf{R}_\mathrm{y}$ as $\mathbf{R}_\mathrm{y}^{[m,n]} = (\mathbf{J}_1 \otimes \mathbf{J}_2)\mathbf{R}_\mathrm{y}(\mathbf{J}_1 \otimes \mathbf{J}_2)^T$, where $\mathbf{J}_1 = [0_{6M_t \times 6(m-1)} \mid \mathbf{I}_{6M_t} \mid 0_{6M_t \times 6(P_\mathrm{t}-m)}]$ and $\mathbf{J}_2 = [0_{6N_r \times 6(n-1)} \mid \mathbf{I}_{6N_r} \mid 0_{6N_r \times 6(P_\mathrm{r}-n)}]$. Now, as the conventional forward-only spatial smoothing, the smoothed covariance matrix $\mathbf{R}_\mathrm{y}^\mathrm{fo}$ can be expressed as

$$\mathbf{R}_\mathrm{y}^\mathrm{fo} = \frac{1}{P_tP_\mathrm{r}} \sum_{m=1}^{P_\mathrm{t}} \sum_{n=1}^{P_\mathrm{r}} \mathbf{R}_\mathrm{y}^{[m,n]} = \tilde{\mathbf{A}}\mathbf{R}_\mathrm{s}^\mathrm{fo}\tilde{\mathbf{A}}^H + \mathbf{R}_\mathrm{z}^\mathrm{fo} \tag{7}$$

where $\tilde{\mathbf{A}} = [\tilde{\mathbf{a}}_{\mathrm{t}_1} \otimes \tilde{\mathbf{a}}_{\mathrm{r}_1}, \ldots, \tilde{\mathbf{a}}_{\mathrm{t}_K} \otimes \tilde{\mathbf{a}}_{\mathrm{r}_K}]$ in which $\tilde{\mathbf{a}}_{\mathrm{t}_k}$ and $\tilde{\mathbf{a}}_{\mathrm{r}_k}$, $\forall\ k = 1, \ldots, K$, represent the first $6M_\mathrm{t}$ and the first $6N_\mathrm{r}$ rows of $\mathbf{a}_{\mathrm{t}_k}$ and $\mathbf{a}_{\mathrm{r}_k}$, respectively; the matrix $\mathbf{R}_\mathrm{s}^\mathrm{fo}$, given in Eq. (8), is the modified and smoothed version of $\mathbf{R}_\mathrm{s}$ in which the modification is performed by the joint transmitting and receiving array spatial phase-shift factors; and $\mathbf{R}_\mathrm{z}^\mathrm{fo}$ is the smoothed noise covariance matrix. The matrix $\mathbf{R}_\mathrm{s}^\mathrm{fo}$ can be expressed as

$$\mathbf{R}_\mathrm{s}^\mathrm{fo} = \frac{1}{P_\mathrm{t}P_\mathrm{r}} \sum_{m=1}^{P_\mathrm{t}} \sum_{n=1}^{P_\mathrm{r}} \mathbf{\Phi}_\mathrm{t}^{m-1}\mathbf{\Phi}_\mathrm{r}^{n-1}\mathbf{R}_\mathrm{s}\mathbf{\Phi}_\mathrm{t}^{1-m}\mathbf{\Phi}_\mathrm{r}^{1-n} \tag{8}$$

where $\mathbf{\Phi}_\mathrm{t} = \mathrm{blkdiag}\{\mathbf{\Phi}_\mathrm{tu}, \mathbf{\Phi}_\mathrm{tp}, \mathbf{\Phi}_\mathrm{tc}\}$ in which $\mathbf{\Phi}_\mathrm{tu} = \mathrm{diag}\{\alpha_1, \ldots, \alpha_{K_\mathrm{u}}\}$, $\mathbf{\Phi}_\mathrm{tp} = \mathrm{diag}\{\alpha_{K_\mathrm{u}+1}, \ldots, \alpha_{K_\mathrm{u}+K_\mathrm{p}}\}$, and $\mathbf{\Phi}_\mathrm{tc} = \mathrm{blkdiag}\{\mathbf{\Phi}_{\mathrm{tc}_1}, \ldots, \mathbf{\Phi}_{\mathrm{tc}_D}\}$ with $\mathbf{\Phi}_{\mathrm{tc}_d} = \mathrm{diag}\{\alpha_{d,1}, \ldots, \alpha_{d,Q_d}\}, \forall\ d = 1, \ldots, D$; and $\mathbf{\Phi}_\mathrm{r} = \mathrm{blkdiag}\{\mathbf{\Phi}_\mathrm{ru}, \mathbf{\Phi}_\mathrm{rp}, \mathbf{\Phi}_\mathrm{rc}\}$ in which $\mathbf{\Phi}_\mathrm{ru} = \mathrm{diag}\{\beta_1, \ldots, \beta_{K_\mathrm{u}}\}$, $\mathbf{\Phi}_\mathrm{rp} = \mathrm{diag}\{\beta_{K_\mathrm{u}+1}, \ldots, \beta_{K_\mathrm{u}+K_\mathrm{p}}\}$, and $\mathbf{\Phi}_\mathrm{rc} = \mathrm{blkdiag}\{\mathbf{\Phi}_{\mathrm{rc}_1}, \ldots, \mathbf{\Phi}_{\mathrm{rc}_D}\}$ with $\mathbf{\Phi}_{\mathrm{rc}_d} = \mathrm{diag}\{\beta_{d,1}, \ldots, \beta_{d,Q_d}\}, \forall\ d = 1, \ldots, D$. The factors α_k ($k = 1, \ldots, K_\mathrm{u}$), $\alpha_{K_\mathrm{u}+p}$ ($p = 1, \ldots, K_\mathrm{p}$) and $\alpha_{d,q}$ ($q = 1, \ldots, Q_\mathrm{d}$) denote the spatial phase-shift between the consecutive subarrays of the transmit array associated with the kth uncorrelated target, the pth partially correlated target, and the qth coherent target in the dth cluster, respectively. Sequentially, β_k, $\beta_{K_\mathrm{u}+p}$, and $\beta_{d,q}$ are the spatial phase-shift factors of the consecutive subarrays of receive array.

The matrix $\mathbf{R}_\mathrm{s}^\mathrm{fo}$ in Eq. (8) is now full-rank, i.e., $\mathrm{rank}(\mathbf{R}_\mathrm{s}^\mathrm{fo}) = K$, subject to satisfying the following conditions:

Condition 1: The coherent targets within the cluster should consist of either different azimuth angles or different elevation angles associated with both the DODs and DOAs.

Condition 2: The total number of subarrays should be greater than the maximum of the targets number in all clusters, i.e., $P_\mathrm{t}P_\mathrm{r} \geq Q$, where $Q = \max(Q_1, \ldots, Q_D)$.

3.3. Validation of the Full-Rank of Smoothed Covariance Matrix

For uncorrelated or partially correlated targets, the reflectivity covariance matrix has a full-rank, i.e., $\mathrm{rank}(\mathbf{R}_\mathrm{u}) = K_\mathrm{u}$ and $\mathrm{rank}(\mathbf{R}_\mathrm{p}) = K_\mathrm{p}$. Thus, the rank deficiency of $\mathbf{R}_\mathrm{s}$ has occurred due to the weaker rank of $\mathbf{R}_\mathrm{c}$, i.e., $\mathrm{rank}(\mathbf{R}_\mathrm{c}) = D < K_\mathrm{c}$, where $K_\mathrm{c} = \sum_{d=1}^{D} Q_d$ with $Q_d \geq 2, \forall\ d = 1, \ldots, D$. Besides, the smoothing does not reduce the rank of $\mathbf{R}_\mathrm{u}$ and $\mathbf{R}_\mathrm{p}$. Therefore, the task is now to show that the rank of $\mathbf{R}_\mathrm{c}^\mathrm{fo}$ is K_c.

Upon substituting $\mathbf{R}_\mathrm{s} = \mathrm{blkdiag}\{\mathbf{R}_\mathrm{u}, \mathbf{R}_\mathrm{p}, \mathbf{R}_\mathrm{c}\}$ in Eq. (8), the segment with only the term $\mathbf{R}_\mathrm{c}$ can be expressed as

$$\mathbf{R}_\mathrm{c}^\mathrm{fo} = \frac{1}{P_\mathrm{t}P_\mathrm{r}} \sum_{m=1}^{P_\mathrm{t}} \sum_{n=1}^{P_\mathrm{r}} \mathbf{\Phi}_\mathrm{tc}^{m-1}\mathbf{\Phi}_\mathrm{rc}^{n-1}\mathbf{R}_\mathrm{c}\mathbf{\Phi}_\mathrm{tc}^{1-m}\mathbf{\Phi}_\mathrm{rc}^{1-n} \tag{9}$$

Further, from the definition of $\mathbf{R}_\mathrm{c} = \mathrm{blkdiag}\{\mathbf{R}_{\mathrm{c}_1}, \ldots, \mathbf{R}_{\mathrm{c}_D}\}$, Eq. (9) can be simplified as

$$\mathbf{R}_\mathrm{c}^\mathrm{fo} = \mathrm{blkdiag}\left\{\mathbf{R}_{\mathrm{c}_1}^\mathrm{fo}, \ldots, \mathbf{R}_{\mathrm{c}_D}^\mathrm{fo}\right\} \tag{10}$$

where

$$\mathbf{R}_{\mathrm{c}_d}^\mathrm{fo} = \frac{1}{P_\mathrm{t}P_\mathrm{r}} \sum_{m=1}^{P_\mathrm{t}} \sum_{n=1}^{P_\mathrm{r}} \mathbf{\Phi}_{\mathrm{tc}_d}^{m-1}\mathbf{\Phi}_{\mathrm{rc}_d}^{n-1}\mathbf{R}_{\mathrm{c}_d}\mathbf{\Phi}_{\mathrm{tc}_d}^{1-m}\mathbf{\Phi}_{\mathrm{rc}_d}^{1-n}, \forall\ d = 1, \ldots, D. \tag{11}$$

Equation (10) shows that $\text{rank}(\mathbf{R}_{\text{c}}^{\text{fo}}) = K_{\text{c}}$, if, and only if, the $\text{rank}(\mathbf{R}_{\text{c}_d}^{\text{fo}}) = Q_d,\ \forall\ d = 1, \ldots, D$. Now, upon substituting $\mathbf{R}_{\text{c}_d} = \sigma^2_{K_{\text{u}}+K_{\text{p}}+d}\boldsymbol{\rho}_d\boldsymbol{\rho}_d^H$ in Eq. (11), $\mathbf{R}_{\text{c}_d}^{\text{fo}}$ can be expressed as

$$\mathbf{R}_{\text{c}_d}^{\text{fo}} = \frac{\sigma^2_{K_{\text{u}}+K_{\text{p}}+d}}{P_{\text{t}}P_{\text{r}}}\sum_{m=1}^{P_{\text{t}}}\sum_{n=1}^{P_{\text{r}}}\boldsymbol{\Phi}_{\text{tc}_d}^{m-1}\boldsymbol{\Phi}_{\text{rc}_d}^{n-1}\boldsymbol{\rho}_d\boldsymbol{\rho}_d^H\boldsymbol{\Phi}_{\text{tc}_d}^{1-m}\boldsymbol{\Phi}_{\text{rc}_d}^{1-n} = \Lambda_d\tilde{\mathbf{B}}_d\Psi_d\tilde{\mathbf{B}}_d^H\Lambda_d^H,\quad \forall\ d = 1, \ldots, D, \tag{12}$$

where $\Lambda_d \triangleq \text{diag}\{\rho_{d,1}, \ldots, \rho_{d,Q_d}\} \in \mathbb{C}^{Q_d\times Q_d}$, $\Psi_d \triangleq \text{diag}\{\frac{\sigma^2_{K_{\text{u}}+K_{\text{p}}+d}}{P_{\text{t}}P_{\text{r}}}, \ldots, \frac{\sigma^2_{K_{\text{u}}+K_{\text{p}}+d}}{P_{\text{t}}P_{\text{r}}}\} \in \mathbb{R}^{P_{\text{t}}P_{\text{r}}\times P_{\text{t}}P_{\text{r}}}$, and $\tilde{\mathbf{B}}_d = (\tilde{\mathbf{B}}_{\text{t}_d} \odot \tilde{\mathbf{B}}_{\text{r}_d})^T \in \mathbb{C}^{Q_d\times P_{\text{t}}P_{\text{r}}}$ in which $\tilde{\mathbf{B}}_{\text{t}_d} = [\tilde{\mathbf{b}}_{\text{t}}(\theta_{\text{t}_{d,1}}, \phi_{\text{t}_{d,1}}), \ldots, \tilde{\mathbf{b}}_{\text{t}}(\theta_{\text{t}_{d,Q_d}}, \phi_{\text{t}_{d,Q_d}})] \in \mathbb{C}^{P_{\text{t}}\times Q_d}$ and $\tilde{\mathbf{B}}_{\text{r}_d} = [\tilde{\mathbf{b}}_{\text{r}}(\theta_{\text{r}_{d,1}}, \phi_{\text{r}_{d,1}}), \ldots, \tilde{\mathbf{b}}_{\text{r}}(\theta_{\text{r}_{d,Q_d}}, \phi_{\text{r}_{d,Q_d}})] \in \mathbb{C}^{P_{\text{r}}\times Q_d}$. Besides, the vectors $\tilde{\mathbf{b}}_{\text{t}}(\theta_{\text{t}_{d,k}}, \phi_{\text{t}_{d,k}})$ and $\tilde{\mathbf{b}}_{\text{r}}(\theta_{\text{r}_{d,k}}, \phi_{\text{r}_{d,k}})$ denote the first P_{t} rows of $\mathbf{b}_{\text{t}}(\theta_{\text{t}_{d,k}}, \phi_{\text{t}_{d,k}})$, and the first P_{r} rows of $\mathbf{b}_{\text{r}}(\theta_{\text{r}_{d,k}}, \phi_{\text{r}_{d,k}})$, respectively. Clearly, from the above definition, $\text{rank}(\Lambda_d) = Q_d$ and $\text{rank}(\Psi_d) = P_{\text{t}}P_{\text{r}}$ provided that $\rho_{d,k} \neq 0,\ \forall\ k = 1, \ldots, Q_d$ and $\sigma^2_{K_{\text{u}}+K_{\text{p}}+d} \neq 0,\ \forall\ d = 1, \ldots, D$, respectively.

The matrices $\tilde{\mathbf{B}}_{\text{t}_d}$ and $\tilde{\mathbf{B}}_{\text{r}_d}$ comprise the Vandermonde structures. Thus, if satisfying either $\theta_{\text{t}_{d,k}} \neq \theta_{\text{t}_{d,p}}$ or $\phi_{\text{t}_{d,k}} \neq \phi_{\text{t}_{d,p}},\ \forall\ k \neq p,\ k, p \in (1, \ldots, Q_d)$, then the $\text{rank}(\tilde{\mathbf{B}}_{\text{t}_d}) = \min(P_{\text{t}}, Q_d)$. Likewise, if satisfying either $\theta_{\text{r}_{d,k}} \neq \theta_{\text{r}_{d,p}}$ or $\phi_{\text{r}_{d,k}} \neq \phi_{\text{r}_{d,p}},\ \forall\ k \neq p,\ k, p \in (1, \ldots, Q_d)$, then the $\text{rank}(\tilde{\mathbf{B}}_{\text{r}_d}) = \min(P_{\text{r}}, Q_d)$. Besides, the DODs and DOAs are different because the system model is bistatic MIMO radar, i.e., $\theta_{\text{t}_{d,k}} \neq \theta_{\text{r}_{d,k}}$ or $\phi_{\text{t}_{d,k}} \neq \phi_{\text{r}_{d,k}},\ \forall\ k = 1, \ldots, Q_d$. Thus, the matrix $\tilde{\mathbf{B}}_d$ consists of $2Q_d$ generators of $\tilde{\mathbf{B}}_{\text{t}_d}$ and $\tilde{\mathbf{B}}_{\text{r}_d}$. This condition assures the rank of $\tilde{\mathbf{B}}_d$ is full, i.e., $\text{rank}(\tilde{\mathbf{B}}_d) = \min(P_{\text{t}}P_{\text{r}}, Q_d)$. This holds for **Condition 1**.

From the matrix form of $\mathbf{R}_{\text{c}_d}^{\text{fo}}$ in Eq. (12), the rank of $\mathbf{R}_{\text{c}_d}^{\text{fo}}$ is Q_d when $P_{\text{t}}P_{\text{r}} \geq Q_d$. Consequently, from Eq. (10), $\text{rank}(\mathbf{R}_{\text{c}}^{\text{fo}}) = K_{\text{c}}$ can be obtained intuitively when we choose $P_{\text{t}}P_{\text{r}} \geq Q$, where $Q = \max(Q_1, \ldots, Q_D)$ with any choice of $P_{\text{t}} \geq 1$ and $P_{\text{r}} \geq 1$. This holds for **Condition 2**.

In the above-said conditions, the first condition can be relaxed, but it restricts more on the minimum subarrays required (i.e., second condition) to attain the full-rank. These are described as the following notes:

Note 1: In the case of monostatic MIMO radar (i.e., DODs and DOAs are identical), the matrix $\tilde{\mathbf{B}}_d$ contains only $P_{\text{t}}+P_{\text{r}}-1$ different elements in each row. Thus, $\text{rank}(\tilde{\mathbf{B}}_d)$ is limited by $\min(P_{\text{t}}+P_{\text{r}}-1, Q_d)$, and $\text{rank}(\mathbf{R}_{\text{c}}^{\text{fo}}) = K_{\text{c}}$ is achieved only when $P_{\text{t}} + P_{\text{r}} - 1 \geq Q$.

Note 2: If $\theta_{\text{t}_{d,k}} = \theta_{\text{t}_{d,p}}$ and $\phi_{\text{t}_{d,k}} = \phi_{\text{t}_{d,p}}$ with satisfying either $\theta_{\text{r}_{d,k}} \neq \theta_{\text{r}_{d,p}}$ or $\phi_{\text{r}_{d,k}} \neq \phi_{\text{r}_{d,p}}\ \forall\ k \neq p,\ k, p = 1, \ldots, Q_d$ and $\forall\ d = 1, \ldots, D$, then the rank of $\tilde{\mathbf{B}}_d = \min(P_{\text{r}}, Q_d)$ which is due to $\text{rank}(\tilde{\mathbf{B}}_{\text{t}_d}) = 1$ and $\text{rank}(\tilde{\mathbf{B}}_{\text{r}_d}) = \min(P_{\text{r}}, Q_d)$. Thus, the $\text{rank}(\mathbf{R}_{\text{c}}^{\text{fo}}) = K_{\text{c}}$ is fulfilled only when $P_{\text{r}} \geq Q$ irrespective of any P_{t}.

Note 3: If $\theta_{\text{r}_{d,k}} = \theta_{\text{r}_{d,p}}$ and $\phi_{\text{r}_{d,k}} = \phi_{\text{r}_{d,p}}$ with satisfying either $\theta_{\text{t}_{d,k}} \neq \theta_{\text{t}_{d,p}}$ or $\phi_{\text{t}_{d,k}} \neq \phi_{\text{t}_{d,p}}\ \forall\ k \neq p,\ k, p = 1, \ldots, Q_d$ and $\forall\ d = 1, \ldots, D$, then the rank of $\tilde{\mathbf{B}}_d = \min(P_{\text{t}}, Q_d)$ as the $\text{rank}(\tilde{\mathbf{B}}_{\text{t}_d}) = \min(P_{\text{t}}, Q_d)$ and $\text{rank}(\tilde{\mathbf{B}}_{\text{r}_d}) = 1$. Thus, $\text{rank}(\mathbf{R}_{\text{c}}^{\text{fo}}) = K_{\text{c}}$ is attained only when $P_{\text{t}} \geq Q$ irrespective of any P_{r}.

3.4. Estimation of the Spatial and Polarization Angles

After obtaining the smoothed covariance matrix as described in Section: 3.2, angles are estimated using the ESPRIT-based method [12]. The algorithmic steps of the overall approach are as follows:

(i) Compute the snapshot covariance matrix of $\mathbf{y}(l)$ in (5) using L snapshots as $\hat{\mathbf{R}}_{\text{y}} = \frac{1}{L}\sum_{l=1}^{L}\mathbf{y}(l)\mathbf{y}^H(l)$.

(ii) Compute the smoothed covariance matrix $\mathbf{R}_{\text{y}}^{\text{fo}}$ by Eq. (7).

(iii) Eigendecompose $\mathbf{R}_{\text{y}}^{\text{fo}}$ for obtaining the signal-subspace $\mathbf{E}_{\text{s}}$ and the noise-subspace $\mathbf{E}_{\text{n}}$.

(iv) Partition $\mathbf{E}_{\text{s}}$ into $\mathbf{E}_{\text{t}} = \mathbf{J}_3\mathbf{E}_{\text{s}}$ and $\mathbf{E}_{\text{r}} = \mathbf{J}_4\mathbf{E}_{\text{s}}$, where $\mathbf{J}_3 = \mathbf{I}_{6M_{\text{t}}} \otimes \mathbf{e}_{q_1}^T$, $q_1 \in (1, \ldots, 6N_{\text{r}})$ in which $\mathbf{e}_{q_1}$ is the q_1th column of $\mathbf{I}_{6N_{\text{r}}}$, and $\mathbf{J}_4 = [0_{6N_{\text{r}}\times 6q_2N_{\text{r}}} \mid \mathbf{I}_{6N_{\text{r}}} \mid 0_{6N_{\text{r}}\times(36M_{\text{t}}N_{\text{r}}-6(q_2+1)N_{\text{r}})}]$, $q_2 \in (0, \ldots, 6M_{\text{t}}-1)$. Further, split $\mathbf{E}_{\text{t}}$ into $\mathbf{E}_{\text{t}1} = \mathbf{J}_5\mathbf{E}_{\text{t}}$ and $\mathbf{E}_{\text{t}2} = \mathbf{J}_6\mathbf{E}_{\text{t}}$, and $\mathbf{E}_{\text{r}}$ into $\mathbf{E}_{\text{r}1} = \mathbf{J}_7\mathbf{E}_{\text{r}}$ and $\mathbf{E}_{\text{r}2} = \mathbf{J}_8\mathbf{E}_{\text{r}}$,

where $\mathbf{J}_5 = [\mathbf{I}_{6(M_\mathrm{t}-1)} \mid 0_{6(M_\mathrm{t}-1),6}]$, $\mathbf{J}_6 = [0_{6(M_\mathrm{t}-1),6} \mid \mathbf{I}_{6(M_\mathrm{t}-1)}]$, $\mathbf{J}_7 = [\mathbf{I}_{6(N_\mathrm{r}-1)} \mid 0_{6(N_\mathrm{r}-1),6}]$, and $\mathbf{J}_8 = [0_{6(N_\mathrm{r}-1),6} \mid \mathbf{I}_{6(N_\mathrm{r}-1)}]$.

(v) Estimate $\{\mathbf{c}_{\mathrm{t}_k}\}_{k=1}^{K}$ as $[\hat{\mathbf{c}}_{\mathrm{t}_1}, \ldots, \hat{\mathbf{c}}_{\mathrm{t}_K}] = \frac{1}{M_\mathrm{t}} \sum_{i=1}^{M_\mathrm{t}} (\tilde{\mathbf{E}}_{\mathrm{t}_i} \mathbf{T}_{\mathrm{cr}}^{-1} \Lambda_\mathrm{t}^{1-i})$, where Λ_t and $\mathbf{T}_{\mathrm{cr}}$ are the eigenvalues and the right-eigenvectors of $\{(\mathbf{E}_{\mathrm{t}1}^H \mathbf{E}_{\mathrm{t}1}^H)^{-1} \mathbf{E}_{\mathrm{t}1}^H \mathbf{E}_{\mathrm{t}2}\}$, respectively, and $\tilde{\mathbf{E}}_{\mathrm{t}_i}$ represents $(6i\text{-}5)$th row to $(6i)$th row of $\mathbf{E}_\mathrm{t}$.

(vi) Compute the cross product between the first three and the conjugate of remaining three components of $\hat{\mathbf{c}}_{\mathrm{t}_k}$ for each $k = 1, \ldots, K$, which obtains $(\hat{u}_{\mathrm{t}_k}, \hat{v}_{\mathrm{t}_k}, \hat{w}_{\mathrm{t}_k}) = (\sin\hat{\theta}_{\mathrm{t}_k} \cos\hat{\phi}_{\mathrm{t}_k},\ \sin\hat{\theta}_{\mathrm{t}_k} \sin\hat{\phi}_{\mathrm{t}_k},\ \cos\hat{\theta}_{\mathrm{t}_k})$. Thus, $\hat{\theta}_{\mathrm{t}_k} = \sin^{-1}(\sqrt{\hat{u}_{\mathrm{t}_k}^2 + \hat{v}_{\mathrm{t}_k}^2})$ and $\hat{\phi}_{\mathrm{t}_k} = \tan^{-1}(\frac{\hat{v}_{\mathrm{t}_k}}{\hat{u}_{\mathrm{t}_k}})$, $k = 1, \ldots, K$.

(vii) From Eq. (2), $\hat{\mathbf{g}}_k \triangleq \begin{bmatrix} \hat{g}_{1_k} \\ \hat{g}_{2_k} \end{bmatrix} = (\mathbf{F}^H(\hat{\theta}_{\mathrm{t}_k}, \hat{\phi}_{\mathrm{t}_k}) \mathbf{F}(\hat{\theta}_{\mathrm{t}_k}, \hat{\phi}_{\mathrm{t}_k}))^{-1} \mathbf{F}^H(\hat{\theta}_{\mathrm{t}_k}, \hat{\phi}_{\mathrm{t}_k}) \hat{\mathbf{c}}_{\mathrm{t}_k}$. Thus, $\hat{\gamma}_{\mathrm{t}_k} = \tan^{-1}(|\frac{\hat{g}_{1_k}}{\hat{g}_{2_k}}|)$ and $\hat{\eta}_{\mathrm{t}_k} = \angle(\frac{\hat{g}_{1_k}}{\hat{g}_{2_k}})$, $k = 1, \ldots, K$.

(viii) For estimating θ_{r_k}, ϕ_{r_k}, γ_{r_k} and η_{r_k}, repeat the steps v, vi, and vii with $\mathbf{E}_\mathrm{r}$, $\mathbf{E}_{\mathrm{r}1}$ and $\mathbf{E}_{\mathrm{r}2}$ instead $\mathbf{E}_\mathrm{t}$, $\mathbf{E}_{\mathrm{t}1}$ and $\mathbf{E}_{\mathrm{t}2}$.

(ix) Let $\hat{\Phi}_\mathrm{t}$ and $\hat{\Phi}_\mathrm{r}$ denote the parameters $\{\hat{\theta}_\mathrm{t}, \hat{\phi}_\mathrm{t}, \hat{\gamma}_\mathrm{t}, \hat{\eta}_\mathrm{t}\}$ and $\{\hat{\theta}_\mathrm{r}, \hat{\phi}_\mathrm{r}, \hat{\gamma}_\mathrm{r}, \hat{\eta}_\mathrm{r}\}$, respectively. Thus, the kth column of $\tilde{\mathbf{A}}$ can be denoted as $\tilde{\mathbf{a}}(\hat{\Phi}_{\mathrm{t}_k}, \hat{\Phi}_{\mathrm{r}_k}) = \tilde{\mathbf{a}}_{\mathrm{t}_k}(\hat{\Phi}_{\mathrm{t}_k}) \otimes \tilde{\mathbf{a}}_{\mathrm{r}_k}(\hat{\Phi}_{\mathrm{r}_k})$, $k = 1, \ldots, K$. From step vi and step vii, the parameters within $\hat{\Phi}_\mathrm{t}$ of a particular target are paired automatically. Likewise, the parameters within $\hat{\Phi}_\mathrm{r}$ of a particular target are also automatically paired. Then, based on the fact that the columns of $\tilde{\mathbf{A}}$ are orthogonal to the columns of $\mathbf{E}_\mathrm{n}$, pairing between $\hat{\Phi}_\mathrm{t}$ and $\hat{\Phi}_\mathrm{r}$ of a particular target can be obtained by finding $f(\hat{\Phi}_{\mathrm{t}_k}, \hat{\Phi}_{\mathrm{r}_p}) \triangleq \tilde{\mathbf{a}}^H(\hat{\Phi}_{\mathrm{t}_k}, \hat{\Phi}_{\mathrm{r}_p}) \mathbf{E}_\mathrm{n} \mathbf{E}_\mathrm{n}^H \tilde{\mathbf{a}}(\hat{\Phi}_{\mathrm{t}_k}, \hat{\Phi}_{\mathrm{r}_p})$, $k, p = 1, \ldots, K$, and selecting the minimum value concerning $\hat{\Phi}_{\mathrm{r}_p}$ for each $\hat{\Phi}_{\mathrm{t}_k}$.

3.5. Complexity Analysis

Computational complexity of the proposed approach depends mainly on the computation of step i, step ii, step iii, DODs estimation (step v–step vii), DOAs estimation, and the pairing between DODs and DOAs (step ix). The complexity of step i, step ii, and step iii is $\mathcal{O}\{(6M)^2(6N)^2L\}$, $\mathcal{O}\{(6M_\mathrm{t})^2(6N_\mathrm{r})^2\}$, and $\mathcal{O}\{(6M_\mathrm{t})^3(6N_\mathrm{r})^3\}$, respectively. The DODs estimation requires the complexity of $\mathcal{O}\{2K^2 6(M_\mathrm{t}-1) + 3K^3 + 7M_\mathrm{t}K^2\}$ for step v, $\mathcal{O}\{6K\}$ for step vi, and $\mathcal{O}\{48K\}$ for step vii. Likewise, DOAs requires the complexity of $\mathcal{O}\{2K^2 6(N_\mathrm{r}-1) + 3K^3 + 7N_\mathrm{r}K^2 + 54K\}$. Finally, pairing between the DODs and DOAs requires $\mathcal{O}\{(36M_\mathrm{t}N_\mathrm{r}(36M_\mathrm{t}N_\mathrm{r} - K) + (36M_\mathrm{t}N_\mathrm{r} - K))K^2\}$.

4. CRAMER-RAO LOWER BOUND

As described the signal model in Section 2, according to [16], the Cramer-Rao bound (CRB) of all parameters to be estimated can be obtained as

$$\mathbf{J} = \frac{\sigma_z^2}{2L} \left[\mathrm{Re}\left(\mathbf{E}^H \Pi_A^\perp \mathbf{E} \oplus \mathbf{R}_s^{\dagger T} \right) \right]^{-1} \tag{13}$$

where σ_z^2 is the noise variance, $\mathbf{E} = [\{\frac{\partial \mathbf{a}_k}{\partial \theta_{\mathrm{t}k}}\}_{k=1}^K, \{\frac{\partial \mathbf{a}_k}{\partial \phi_{\mathrm{t}k}}\}_{k=1}^K, \ldots, \{\frac{\partial \mathbf{a}_k}{\partial \eta_{\mathrm{r}k}}\}_{k=1}^K]$, $\Pi_A^\perp = \mathbf{I}_{36MN} - \mathbf{A}(\mathbf{A}^H\mathbf{A})^{-1}\mathbf{A}^H$, and $\mathbf{R}_s^\dagger = 1_8 \otimes \mathbf{R}_s$ in which 1_8 is 8×8 unit matrix. The root CRB of particular parameter $\psi \in (\theta_\mathrm{t}, \phi_\mathrm{t}, \gamma_\mathrm{t}, \eta_\mathrm{t}, \theta_\mathrm{r}, \phi_\mathrm{r}, \gamma_\mathrm{r}, \eta_\mathrm{r})$ can be obtained as

$$\mathrm{CRB}(\psi) = \sqrt{\frac{1}{K} \sum_{k=p+1}^{K} [\mathbf{J}]_{k,k}} \tag{14}$$

where $p = 0, K, 2K, 3K, 4K, 5K, 6K$ and $7K$ for $\psi = \theta_\mathrm{t}, \phi_\mathrm{t}, \gamma_\mathrm{t}, \eta_\mathrm{t}, \theta_\mathrm{r}, \phi_\mathrm{r}, \gamma_\mathrm{r}$, and η_r, respectively.

5. SIMULATION RESULTS

This section presents the Monte-Carlo simulations to examine the effectiveness of the proposed approach. For all simulations, we consider $M = N = 10$ EVSs with spacing $d_{\rm t} = d_{\rm r} = \lambda/2$, $P_{\rm t} = P_{\rm r} = 6$ subarrays for performing the smoothing, Hadamard codes of length $P = 128$ for transmission of the orthogonal waveforms, $q_1 = 2$ in $\mathbf{J}_3$ and $q_2 = 1$ in $\mathbf{J}_4$ for partitioning $\mathbf{E}_{\rm s}$, and the noise is complex Gaussian with zero mean. All simulations are executed over $M_{\rm c} = 500$ Monte-Carlo runs.

In the first simulation, shown in Fig. 2, we describe the advantage of both spatial and polarization angle estimation by evaluating the resolution probability (RP). The RP for resolving a target concerning with the DODs/DOAs is computed statistically from the successful trials, which accounts when the absolute estimation error is below a threshold δ. The threshold δ for multiple parameters of DOD/DOA estimation is defined by

$$\delta = \min\left\{\sqrt{(\Delta\boldsymbol{\Theta}_{k,p})^T\Delta\boldsymbol{\Theta}_{k,p}},\ k \neq p,\ k,p = 1,\ldots,K\right\} \tag{15}$$

where $\Delta\boldsymbol{\Theta}_{k,p} = (\boldsymbol{\Theta}_k - \boldsymbol{\Theta}_p)/(2\sqrt{P})$ in which $\boldsymbol{\Theta}_k = [\theta_k, \phi_k, \gamma_k, \eta_k]^T$ with $P = 4$ (i.e., the method estimates four different parameters of DODs/DOAs). If a method estimates only the elevation angle, then $\boldsymbol{\Theta}_k = \theta_k$ and $P = 1$. Thus, $\delta = \min\{\frac{|\theta_k - \theta_p|}{2}$, for $k \neq p$, $k,p = 1,\ldots,K\}$. For the evaluation of Fig. 2, we consider $L = 100$ snapshots, signal to noise ratio (SNR) is 5 dB, and $K = 3$ coherent targets (i.e., $K_{\rm u} = 0, K_{\rm p} = 0, K_{\rm c} = 3$). The reflectivities of the targets are chosen as $\mathbf{s}_{\rm c}(l) = s_1(l)\boldsymbol{\rho}_1$, where $s_1(l)$ is generated by the complex Gaussian with zero-mean and unit-variance and $\boldsymbol{\rho}_1 = [1,\ 0.2 + 0.84j,\ 0.4 + 0.7j]^T$.

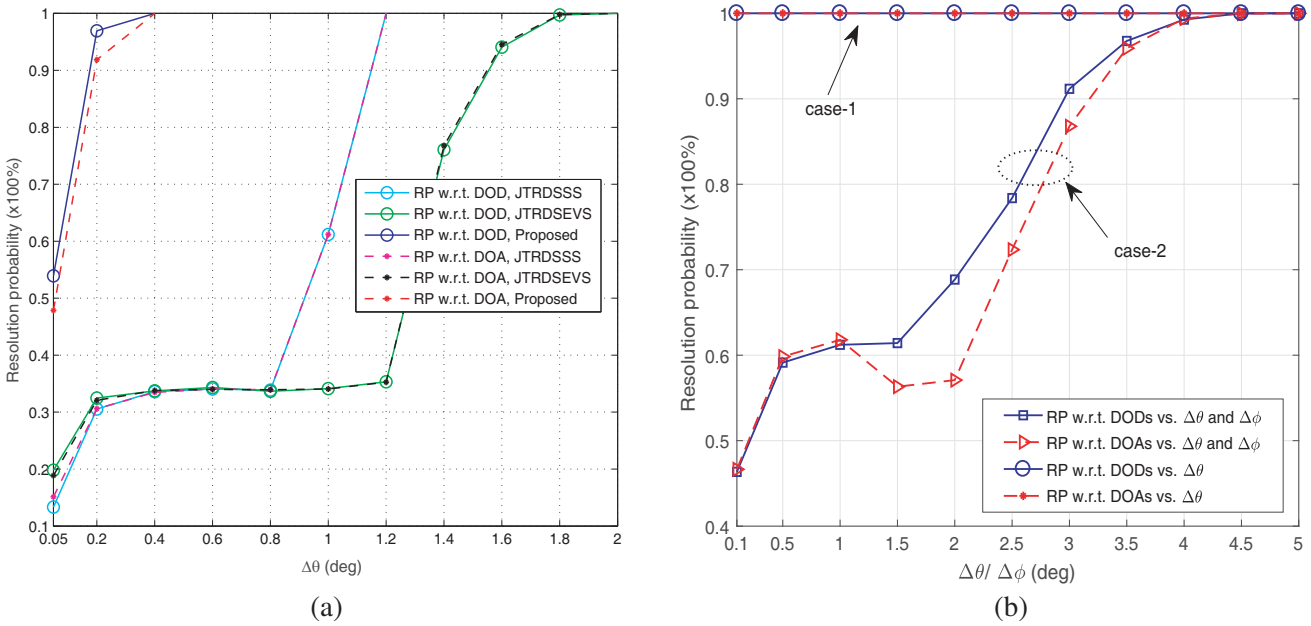

Figure 2. Performance of the targets resolving probability versus the angular deviation. (a) RP based on elevation angle vs $\Delta\theta$. (b) RP based on all parameters vs $\Delta\theta$ and $\Delta\phi$.

The methods proposed in [8] (denoted as JTRDS-SS) and in [9] (denoted as JTRDS-EVS) estimate only the elevation angles of targets. Thus, for measuring and comparing the RP, threshold δ is constructed based on a single parameter that is elevation angle, and the performance is depicted in Fig. 2(a). In Fig. 2(a), RP is computed at each value of $\Delta\theta$ ranging from 0.05° to 2°. The target postures are taken as $\boldsymbol{\theta}_{\rm t} = (30° - \Delta\theta, 30°, 30° + \Delta\theta)$, $\boldsymbol{\phi}_{\rm t} = (14°, 54°, 40°)$, $\boldsymbol{\gamma}_{\rm t} = (70°, 50°, 30°)$, $\boldsymbol{\eta}_{\rm t} = (35°, 11°, 27°)$, $\boldsymbol{\theta}_{\rm r} = (25° - \Delta\theta, 25°, 25° + \Delta\theta)$, $\boldsymbol{\phi}_{\rm r} = (12°, 24°, 36°)$, $\boldsymbol{\gamma}_{\rm r} = (15°, 35°, 58°)$, and $\boldsymbol{\eta}_{\rm r} = (59°, 21°, 39°)$. The number of scalar sensors of the method JTRDS-SS is chosen as $M = N = 35$, which ensures that the

dimension of $\mathbf{R}_{\mathrm{y}}^{\mathrm{fo}}$ is equal for all the methods under $P_{\mathrm{t}} = P_{\mathrm{r}} = 6$. The results in Fig. 2(a) signify that the proposed approach exhibits outstanding performance.

In Fig. 2(b), the threshold δ is constructed based on all four parameters and depicts the RP performance versus $\Delta\theta$ (case-1) and both $\Delta\theta$ and $\Delta\phi$ (case-2). For case-1, the target postures are same as in Fig. 2(a). For case-2, $\boldsymbol{\theta}_{\mathrm{t}} = (30^\circ - \Delta\theta, 30^\circ, 30^\circ + \Delta\theta)$, $\boldsymbol{\theta}_{\mathrm{r}} = (25^\circ - \Delta\theta, 25^\circ, 25^\circ + \Delta\theta)$, $\boldsymbol{\phi}_{\mathrm{t}} = (35^\circ - \Delta\phi, 35^\circ, 35^\circ + \Delta\phi)$, $\boldsymbol{\phi}_{\mathrm{r}} = (40^\circ - \Delta\phi, 40^\circ, 40^\circ + \Delta\phi)$, and the remaining all parameter values are same as in Fig. 2(a). From case-1, 100% RP is achieved at $\Delta\theta = 0.1^\circ$ (even true at $\Delta\theta = 0^\circ$), which signifies that the proposed approach resolves the targets having the same elevation angles. Furthermore, from case-2, the proposed approach resolves the targets even if they are closely located in both azimuth and elevation angles, e.g., 99% RP is attained at $\Delta\theta, \Delta\phi = 4^\circ$. This attainment is due to the utilization of polarization angle estimation. Thus, both spatial and polarization angle estimations are highly

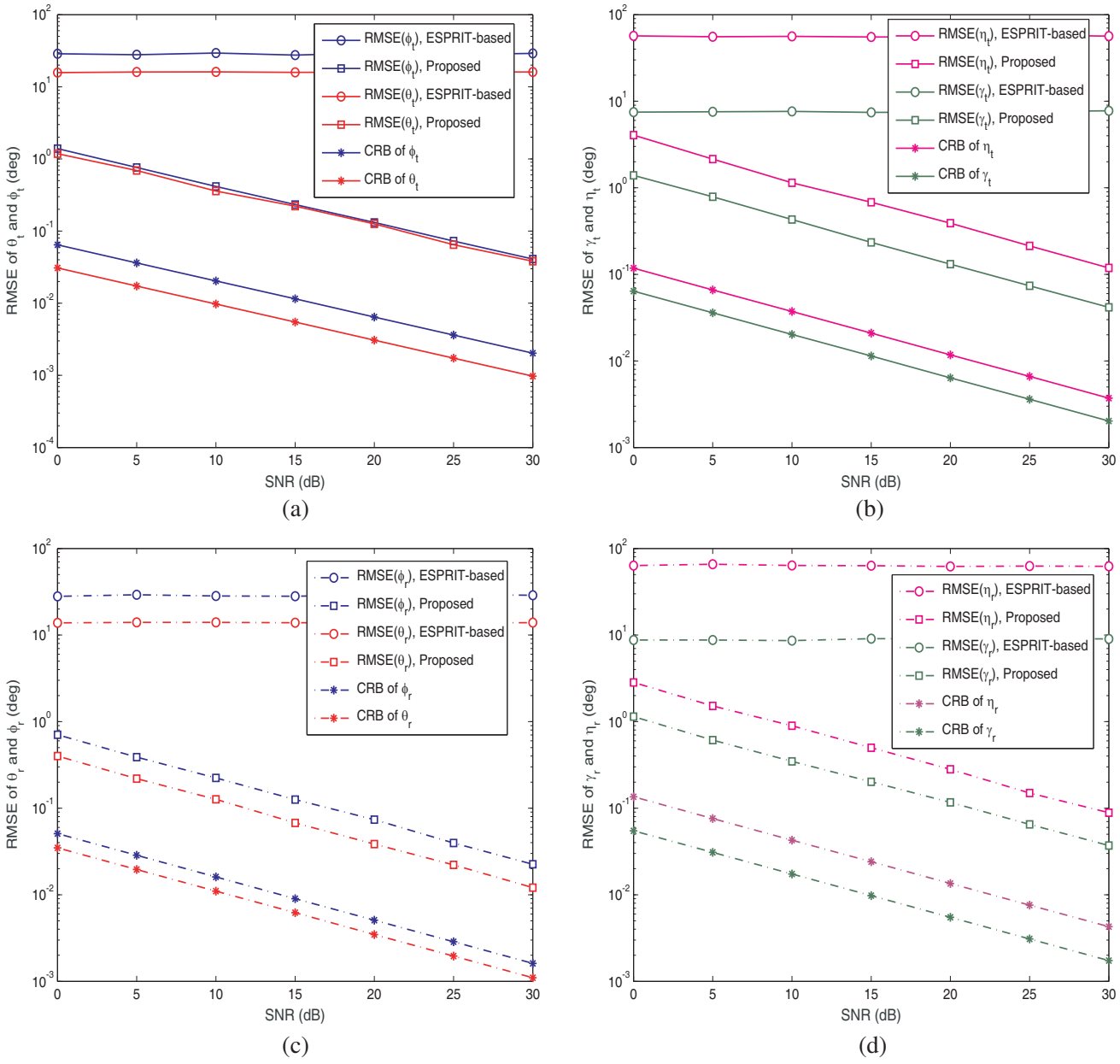

Figure 3. RMSE of the spatial and polarization angles of DOD and DOA. (a) RMSE of θ_t and ϕ_t. (b) RMSE of γ_t and η_t. (c) RMSE of θ_r and ϕ_r. (d) RMSE of γ_r and η_r.

essential for resolving the closely located targets.

Hereafter, in all the simulations, we consider $L = 300$ snapshots and $K = 6$ targets in which $K_{\mathrm{u}} = 1$, $K_{\mathrm{p}} = 2$, and $D = 1$ cluster with $K_{\mathrm{c}} = 3$. The concerning reflectivities $s_1(l)$, $\mathbf{s}_{\mathrm{p}}(l) = [s_2(l), s_3(l)]^T$, and $\mathbf{s}_{\mathrm{c}}(l) = s_4(l)\boldsymbol{\rho}_1$ are generated by the complex Gaussian with zero mean and unit variance. For partially correlated targets, the correlation coefficient between $s_2(l)$ and $s_3(l)$ is set to 0.5. For coherent targets, the correlation coefficient is set to one with $\boldsymbol{\rho}_1 = [1, 0.2 + 0.84j, 0.4 + 0.7j]^T$. The sequential angles are taken as $\boldsymbol{\theta}_t = (10°, 50°, 45°, 40°, 25°, 20°)$, $\boldsymbol{\phi}_t = (12°, 24°, 36°, 30°, 52°, 48°)$, $\boldsymbol{\gamma}_t = (70°, 50°, 30°, 20°, 40°, 60°)$, $\boldsymbol{\eta}_t = (35°, 11°, 27°, 51°, 19°, 43°)$, $\boldsymbol{\theta}_r = (8°, 17°, 22°, 30°, 42°, 46°)$, $\boldsymbol{\phi}_r = (14°, 54°, 40°, 50°, 23°, 28°)$, $\boldsymbol{\gamma}_r = (15°, 35°, 58°, 75°, 45°, 25°)$, and $\boldsymbol{\eta}_r = (59°, 21°, 39°, 49°, 69°, 79°)$.

In the second simulation, shown in Fig. 3, root-mean-squared-error (RMSE) is measured and compared with the ESPRIT-based method [12] and the root CRB. The RMSE is defined by

$$\mathrm{RMSE} = \sqrt{\frac{1}{M_{\mathrm{c}}K}\sum_{k=1}^{K}\sum_{i=1}^{M_{\mathrm{c}}}\left(\psi_k - \hat{\psi}_{k,i}\right)^2} \tag{16}$$

where $\hat{\psi}_{k,i}$ denotes the estimate of $\psi_k \in (\theta_{\mathrm{t}_k}, \phi_{\mathrm{t}_k}, \gamma_{\mathrm{t}_k}, \eta_{\mathrm{t}_k}, \theta_{\mathrm{r}_k}, \phi_{\mathrm{r}_k}, \gamma_{\mathrm{r}_k}, \eta_{\mathrm{r}_k})$ in the ith Monte-Carlo run, and M_{c} denotes the total number of Monte-Carlo runs. The results in Fig. 3 signify that the performance of the proposed approach follows the root CRB whereas performance of the ESPRIT-based method [12] is unsatisfactory, and constant floor occurs even at high SNR.

The next simulation illustrates the precision performance of the angle estimates using the scatter plot shown in Fig. 4. In Fig. 4(a), the estimated angles are spread randomly over the entire region. Thus, from Figs. 3 and 4(a), we signify that the ESPRIT-based method [12] fails to resolve the coherent

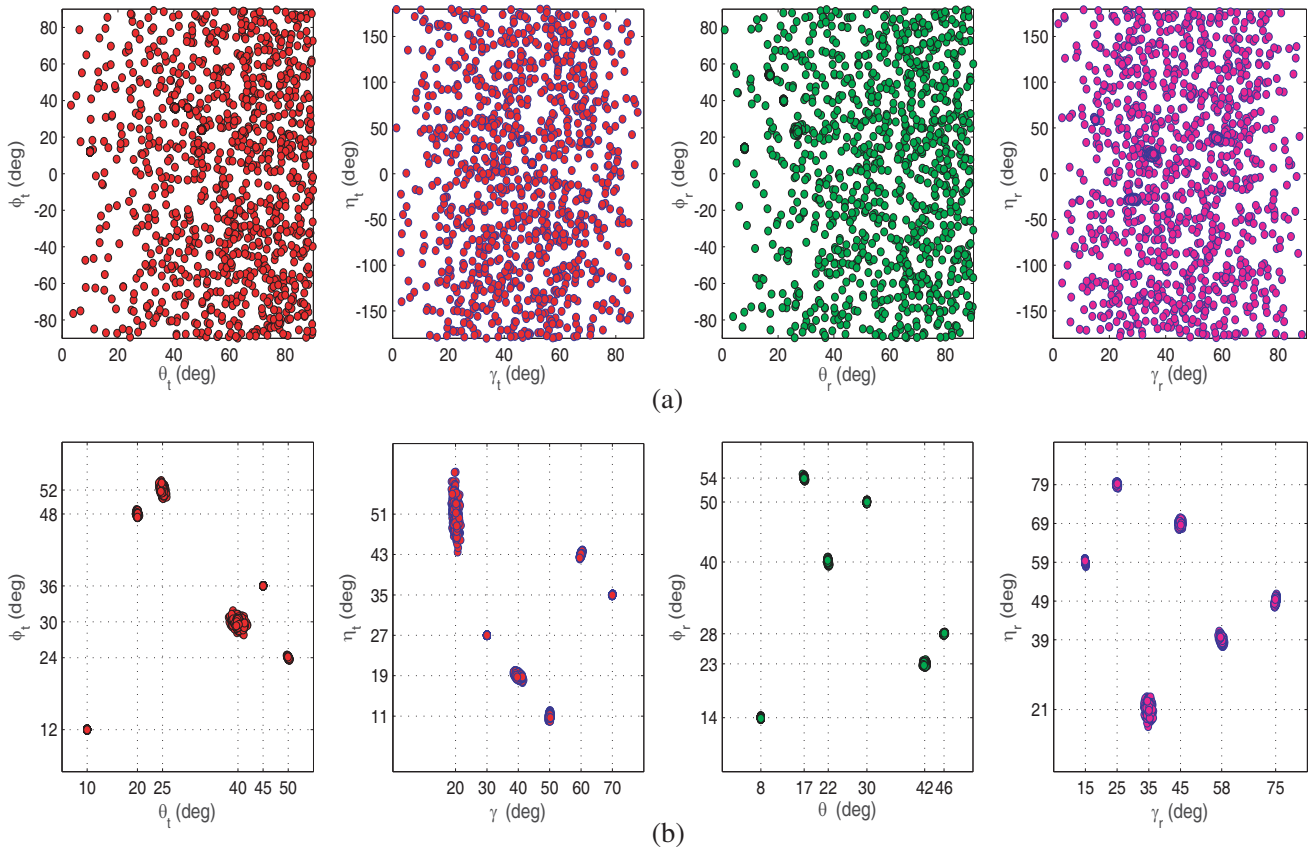

Figure 4. Scatters of the spatial and polarization angle estimates of DODs and DOAs. (a) ESPRIT-based method. (b) Proposed approach.

or mixed targets. However, in the proposed method shown in Fig. 4(b), the estimated angles of a particular target are close to the actual value.

The final simulation, shown in Fig. 5, illustrates the conceivable three-dimensional stem plots for visualizing the pair-matching among all the eight parameters. For clearly identifying the location of the projected stems on the horizontal plane, grid-lines are highlighted only for the actual values of the concerning parameters. From the illuminated results in Fig. 5, one can notice that the spatial and polarization angles of DODs and DOAs of all targets are paired precisely.

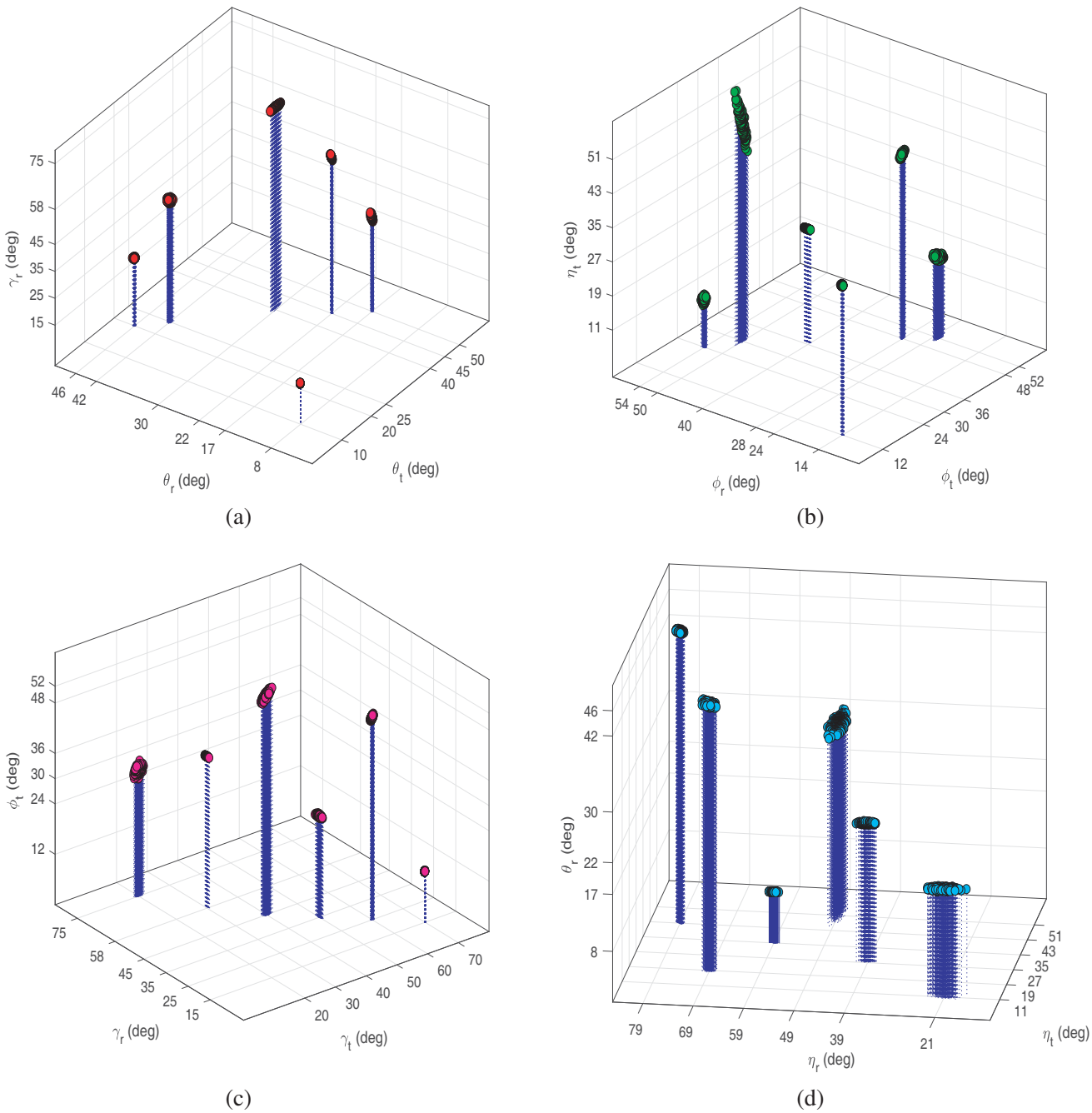

Figure 5. Pair-matching among all the eight parameters. (a) Pairing of θ_t, θ_r and γ_r. (b) Pairing of ϕ_t, ϕ_r and η_t. (c) Pairing of γ_t, γ_r and ϕ_t. (d) Pairing of η_t, η_r and θ_r.

6. CONCLUSION

This paper constructs a more relevant scenario to the practical one that comprises a combination of uncorrelated, partially correlated, and the groups of coherent targets. In this scenario, we examine the importance of estimating multiple parameters like azimuth, elevation, and polarization angles for localization of the targets in bistatic MIMO radar. The proposed approach can locate any number of targets with pair-matching among all the parameters. Consequently, the proposed approach is practicable for the application where localization of the targets with multiple parameters estimations is essential.

REFERENCES

1. Li, J. and P. Stoica, "MIMO radar with colocated antennas," *IEEE Signal Processing Magazine*, Vol. 24, No. 5, 106–114, 2007.
2. Zhang, X., X. Gao, G. Feng, and D. Xu, "Blind joint DOA and DOD estimation and identifiability results for MIMO radar with different transmit/receive array manifolds," *Progress In Electromagnetics Research B*, Vol. 18, 101–119, 2009.
3. Chen, H. W., D. Yang, H. Q. Wang, X. Li, and Z. W. Zhuang, "Direction finding for bistatic MIMO radar using EM maximum likelihood algorithm," *Progress In Electromagnetics Research*, Vol. 141, 99–116, 2013.
4. Zheng, G. and B. Chen, "Unitary dual-resolution ESPRIT for joint DOD and DOA estimation in bistatic MIMO radar," *Multidimensional Systems and Signal Processing*, Vol. 26, 159–178, 2015.
5. Jiang, H., J. K. Zhang, and K. M. Wong, "Joint DOD and DOA estimation for bistatic MIMO radar in unknown correlated noise," *IEEE Transactions on Vehicular Technology*, Vol. 64, No. 11, 5113–5125, 2015.
6. Wena, F., X. Xiong, J. Su, and Z. Zhang, "Angle estimation for bistatic MIMO radar in the presence of spatial colored noise," *Signal Processing*, Vol. 134, 261–267, 2017.
7. Chen, H., X. Zhang, Y. Bai, and J. Ma, "Direction finding for bistatic MIMO radar with non-circular sources," *Progress In Electromagnetics Research M*, Vol. 66, 173–182, 2018.
8. Zhang, W., W. Liu, J. Wang, and S. Wu, "Joint transmission and reception diversity smoothing for direction finding of coherent targets in MIMO radar," *IEEE Journal of Selected Topics in Signal Processing*, Vol. 8, No. 1, 115–124, 2014.
9. Srinivasarao, C. and P. Palanisamy, "DOD and DOA estimation using the spatial smoothing in MIMO radar with the EmV sensors," *Multidimensional Systems and Signal Processing*, Vol. 29, No. 4, 1241–1253, 2018.
10. Chen, C. and X. Zhang, "A low-complexity joint 2D-DOD and 2D-DOA estimation algorithm for MIMO radar with arbitrary arrays," *International Journal of Electronics*, Vol. 100, No. 10, 1455–1469, 2013.
11. Xia, T.-Q., "Joint diagonalization based 2D-DOD and 2D-DOA estimation for bistatic MIMO radar," *Signal Processing*, Vol. 116, 7–12, 2015.
12. Srinivasarao, C. and P. Palanisamy, "2D-DOD and 2D-DOA estimation using the electromagnetic vector sensors," *Signal Processing*, Vol. 147, 163–172, 2018.
13. Ye, Z., Y. Zhang, and C. Liu, "Direction-of-arrival estimation for uncorrelated and coherent signals with fewer sensors," *IET Microwaves, Antennas and Propagation*, Vol. 3, No. 3, 473–482, 2009.
14. Liu, F., J. Wang, C. Sun, and R. Du, "Spatial differencing method for DOA estimation under the coexistence of both uncorrelated and coherent signals," *IEEE Transactions on Antennas and Propagation*, Vol. 60, No. 4, 2052–2062, 2012.
15. Qin, S., Y. D. Zhang, and M. G. Amin, "DOA estimation of mixed coherent and uncorrelated targets exploiting coprime MIMO radar," *Digital Signal Processing*, Vol. 61, 26–34, 2017.
16. Shi, J., G. Hu, X. Zhang, and S. Jin, "Smoothing matrix set-based MIMO radar coherent source localisation," *International Journal of Electronics*, Vol. 105, No. 8, 1345–1357, 2018.